Turbulence in Flowing Soap Films: Velocity, Vorticity, and Thickness Fields

Michael Rivera,* Peter Vorobieff, and Robert E. Ecke
Condensed Matter & Thermal Physics Group and Center for Nonlinear Studies, Los Alamos National Laboratory, Los Alamos, New Mexico 87545
(Received 3 March 1998)

We report experimental measurements of the velocity, vorticity, and thickness fields of turbulent flowing soap films using a modified particle-image velocimetry technique. These data yield the turbulent energy and enstrophy of the two-dimensional flows with microscale Reynolds numbers of about 100 and demonstrate the effects of compressibility arising from variations in film thickness. Despite the compressibility of the flow, real-space correlations of velocity, vorticity, and enstrophy flux are consistent with theoretical predictions for two-dimensional turbulence. [S0031-9007(98)06858-6]

PACS numbers: 47.27.Gs, 67.40.Vs, 92.60.Ek

Soap films have been a test bed for two-dimensional (2D) turbulence since Couder proposed their use and conducted a series of experiments characterizing their properties [1]. The fascination with two-dimensional turbulence [2] comes from its seeming simplicity relative to turbulence in three dimensions and from possible application in geophysical problems, where two-dimensional approximations are commonly made. The theory of 2D incompressible turbulence was first developed by Batchelor [3] and Kraichnan [4] and makes distinct predictions for the behavior of statistical quantities characterizing the flow. One of the most directly testable predictions arising from the statistical theories is the scaling of turbulent velocity fluctuations. In 2D turbulence, the scaling of kinetic energy E for length scales smaller than the injection scale is controlled by the cascade of enstrophy Ω (mean-square vorticity) giving rise to a k^{-3} energy spectrum and a k^{-1} scaling of the enstrophy.

Experiments with soap films have employed single-point probes of velocity to characterize the velocity field. These temporal measurements, used in conjunction with the Taylor frozen-turbulence hypothesis, yield an approximate k^{-3} scaling range of energy $E(k)$ [5,6] consistent with the enstrophy cascade picture of 2D turbulence. Direct measurements of vorticity would, however, more clearly establish that the enstrophy cascade is indeed there. Recently, measurements of vorticity using several one-point probes [7] found an enstrophy scaling of $k^{-1.8}$, quite different from the k^{-1} scaling predicted by theory. This difference in scaling was attributed to possible compressibility effects, raising the question as to how well these films are actually described by the 2D incompressible Navier-Stokes equation. Thickness variations are present in these films when a grid or rod is inserted in the flow to create turbulence [1,8] and provide a useful visualization mechanism for soap films. There has been, however, no quantitative investigation of thickness fluctuations to determine if the fluctuations are merely created by the inserted grid and advected downstream, or if they can be created by finite divergence in the flow. Further, the effect of possible compressibility on the statistics of 2D turbulence remains a mystery.

Although single-point measurements employed to date are valuable probes of the state of turbulent soap-film flows, they have some important limitations. It is known, for example, from numerical simulations [9] that the overall flow structure consisting primarily of vortices is vital in understanding the nature of the 2D turbulent flow. Thus, it is important in physical experiments to measure, if possible, the velocity and vorticity *fields* as opposed to single-point probes of velocity. Such measurements, combined with simultaneous measurements of film thickness, would elucidate much more fully the nature of turbulence in quasi-2D flowing soap films.

We used particle image velocimetry (PIV) to measure turbulent velocity and vorticity fields produced by a grid inserted in a flowing soap film. We also obtained semi-quantitative measurements of film thickness (Fig. 1) from the intensity of the light scattered by the seeding particles. We demonstrate that film thickness and fluid vorticity are strongly coupled, that film-thickness fluctuations are not small on the scale of total film thickness, and that the flow is significantly compressible with mean-square divergence about 10%–20% of the mean-square vorticity. We also compute the ensemble-averaged real-space two-point structure functions of velocity, vorticity, and enstrophy flux. We compare the scaling of these quantities with theoretical predictions and find that they are roughly consistent with 2D incompressible turbulence theory despite the contributions of compressibility and the moderate microscale Reynolds number $R_\lambda \approx 100$. This study significantly extends our understanding of turbulent flows in soap films and sets particular challenges for future research.

The experimental apparatus consisted of a reservoir at the bottom and an injection nozzle at the top, supported by a frame which could be tilted at an arbitrary angle with respect to vertical. The design of the soap-film channel itself follows closely the descriptions of Kellay *et al.* [6,7] and Rutgers *et al.* [10]. Two 0.5 mm diameter nylon wires were stretched from top to bottom to create

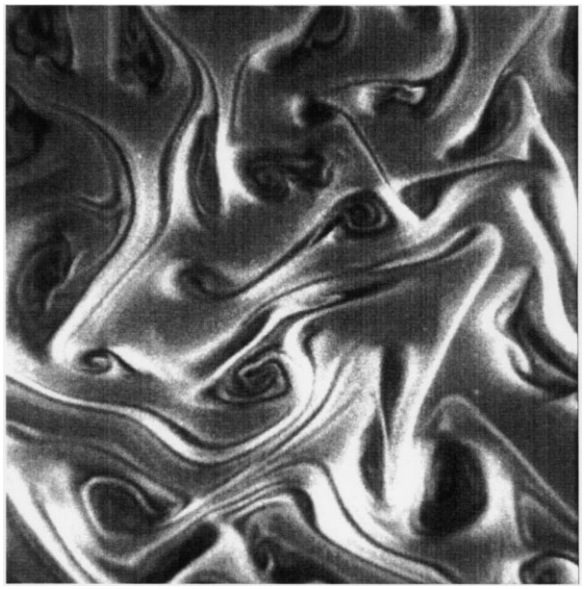

FIG. 1. Thickness field (dark is thinner, light is thicker; peak variation of ±35% mean thickness) of a 2.5 cm × 2.5 cm portion of the film just behind the grid.

a parallel channel 6 cm wide and 1.2 m long. The soap solution, 2% commercial soap in water, was continuously recirculated to the top of the channel at a flow rate of 1.7 ml/s. The channel was tilted at 8° with respect to horizontal to produce thicker films which were more turbulent than vertical, thinner films at the same flow velocity. The turbulent flow was produced by a grid of cylindrical teeth—2.7 mm diameter metal cylinders spaced 3 mm apart—inserted into the flow. The mean flow velocity v_m was 1.05 m/s and the fluid viscosity is estimated to be about 0.03 cm^2/s, less than that for the thinner films in vertical channels [10] but consistent with films of comparable thickness [1].

To obtain measurements of the fluid velocity $\mathbf{v}(x, y)$, titanium dioxide particles with average size 0.2 ± 0.1 μm were mixed with the soap solution at a volume concentration of 5×10^{-5}. The film was illuminated by two 360 mJ/pulse flash lamps, each of which had a pulse duration of about 2 μs. The adjustable delay between the lamps, determined by v_m, was 50 to 200 μs. The flashes illuminated the film from behind at an angle of about 45°, and a 1007 × 1018 pixel CCD camera recorded images of the film. The particles were sufficiently small that diffuse light scattering provided a measure of film thickness proportional to scattered light intensity. We calibrated this proportionality using a test sample such that direct measurement of the film thickness from the volume flow rate yields a film thickness $h = 27$ μm, whereas the calibration gives 30 ± 3 μm. Diffraction spots from individual particles, visible in the video images, were interrogated using a commercial PIV analysis package [11].

The application of PIV to flowing soap films posed several limitations when compared to typical PIV applications. First, the particles must be small compared with the film thickness. For a reasonable area in the film channel of order 1 cm^2, the size of a single pixel corresponds to 6–12 μm, larger than the particle size. Thus, the particle position was known only up to ±0.5 pixels as opposed to the subpixel resolution obtainable for particles larger than the pixel resolution. Second, the high speed of the flow necessitated using single-frame double exposures which leads to ambiguity in the time ordering. The second problem is alleviated by the strong mean flow of the film but the first is intrinsic to soap films. Despite this limitation, we were able to obtain reliable velocity fields with a physical grid spacing of 200 μm. A third problem is that the characteristic time of structure evolution is much shorter than our frame spacing so we are unable to resolve the dynamics of the vortices. This is not an issue for the statistical analysis presented here.

From the simultaneous thickness and velocity measurements, we obtain a quantitative characterization of the instantaneous fields on discrete 60 × 61 grids. In Fig. 2a, the velocity vectors with v_m subtracted are shown for flow 5 cm behind the grid. Two large vortices are visible in the image which shows a part of the flow with an area of about 1.5 cm^2. The z component of vorticity, computed from the velocity using finite differences, is shown in Fig. 2b for the data in Fig. 2a. We also compute the divergence of the velocity field to check for effective 2D compressibility. The thickness field $h(x, y)$ was obtained directly from light-scattering data with some digital processing to remove inhomogeneities in background lighting and fine-scale noise in the image. The thickness field corresponding to the velocity and vorticity fields in Figs. 2a and 2b is shown in Fig. 2c. There is a clear correlation between vorticity and thickness which we discuss below.

The turbulence we describe is decaying downstream owing to internal dissipation and external air drag. A recent numerical simulation [12] for a range of microscale Reynolds number R_λ gives a good overview of decaying 2D turbulence [3]. To compare with theory and to evaluate the importance of compressibility, we perform ensemble averages over ten different images at several downstream locations to obtain the energy $E = \langle v^2 \rangle$, the enstrophy $\Omega = \langle \omega^2 \rangle$, the mean-square divergence $D = \langle (\nabla \cdot \mathbf{v})^2 \rangle$, and the relative standard deviation of thickness $\langle \delta h^2 \rangle^{1/2} / \langle h \rangle$. These quantities are plotted in Fig. 3 as a function of time ($t = d/v_m$) normalized by the initial value of root-mean-square vorticity ω_0 following Chasnov [12]. The quantities E, Ω, and D are normalized by their values 1 cm behind the rod and correspond to the left axis, whereas the thickness fluctuations correspond to the right axis. The error bars for E are estimated at 1%–2%, those for Ω and D are about 5% owing to finite difference errors, and the uncertainty in relative thickness is less than 5%.

The magnitude of effective 2D compressibility of the film is roughly measured by the ratio D/Ω which ranges

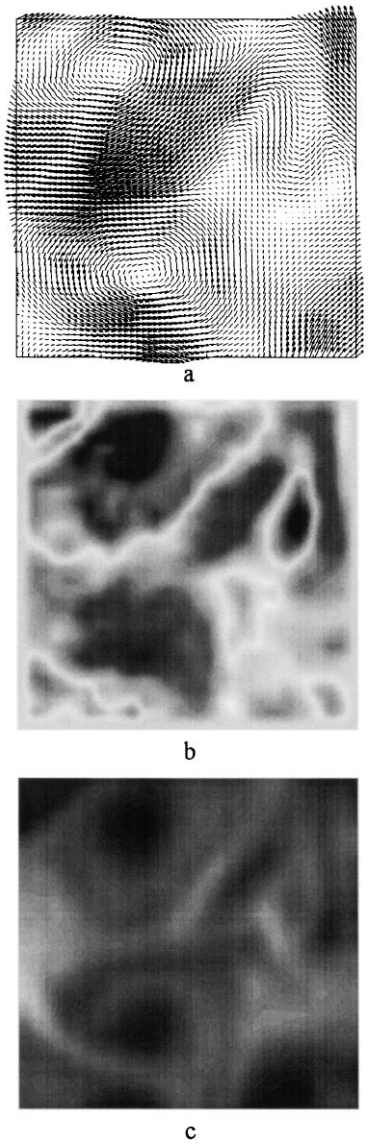

FIG. 2. (a) Velocity vectors, (b) vorticity magnitude (dark is maximum, light is zero), and (c) film thickness (dark is thinner, light is thicker) for $l = 5$ cm downstream from the grid. The gray scale is linear with full scale variation in thickness of $\pm 50\%$. The spatial dimensions are 1.2 cm $\times$ 1.2 cm.

between 0.1 and 0.2. Thus, we see that compressibility is not negligible for these films although it is not so large as to be obviously important. The relative compressibility does not appear to decay downstream, but both Ω and D decrease rapidly with downstream distance. The less rapid decay of E is consistent with the 2D turbulence picture that Ω decays faster than E [3,12] but the data are not sufficient for a quantitative comparison.

These quantities provide information to evaluate a Taylor-microscale Reynolds number $R_\lambda \equiv v_{\mathrm{rms}}\lambda/\nu$, where the Taylor microscale is $\lambda = (E/\Omega)^{1/2}$, $v_{\mathrm{rms}} = \sqrt{E}$, and we use $\nu = 0.03$ cm^2/s. λ and R_λ increase downstream owing to the coarsening represented in Fig. 1 from 0.6 to 1.2 mm and from 70 to 140, respectively.

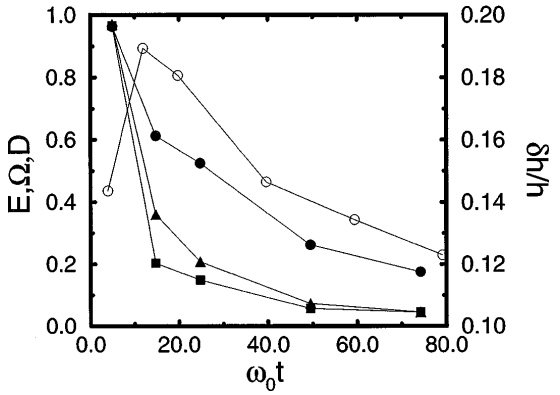

FIG. 3. Decay of normalized E/E_0 (•), Ω/Ω_0 (■), D/D_0 (▲), and $\delta h/h$ (∘) with normalized time $\omega_0 t$. Lines are guides to the eye.

This range of R_λ puts our system into the "high" Reynolds number range, as defined in numerical simulations [12], where turbulent scaling is observed but is not in the very large R_λ limit.

The thickness-fluctuation data can now be interpreted in terms of advection by the velocity field and by compressibility. The strong correlation demonstrated in Fig. 2 between vorticity and film thickness—regions of high vorticity (dark) correspond closely to regions of low film thickness (dark)—is present immediately behind the comb and persists downstream without noticeable deterioration. This implies that film thickness and vorticity are initially correlated presumably because fluid around each comb tooth is wrapped around shedding vortices resulting in thin vortex centers with thick outer edges. The persistence of this correlation indicates that film thickness and vorticity are advected by the flow in roughly the same way, consistent with the picture that thickness is advected like a passive scalar.

This is not the whole story, however, because thickness variations should begin to decay immediately downstream from the rod owing to the restoring force of surface tension [8], whereas the data in Fig. 3 show that $\delta h/h$ initially increases before decaying downstream. This can be understood qualitatively as arising from compressibility. Whereas surface tension will tend to smooth out the surface and reduce average height variations, increases in thickness variation can only arise from the flow of thickness as a result of finite compressibility. For example, flow from the core of vortices will pile up thickness at the edges while thinning the cores, thereby enhancing mean-square thickness variations. Thus, the simplest explanation for our results is that thickness is advected like a passive scalar but in a *compressible* medium so that a term like $h\nabla \cdot \mathbf{v}$ needs to be retained in the hydrodynamics equation for the thickness field.

Despite our evidence that compressibility is not negligible, the flow shows many qualitative characteristics of 2D incompressible turbulence: the coarsening of vortex

size shown in Fig. 1 and the more rapid decay of Ω relative to E (Fig. 3). To evaluate the correspondence with statistical theories of 2D incompressible turbulence, we compute the two-point structure functions. We choose real-space analysis because our relatively small grid of velocity and vorticity vectors makes analysis in Fourier space problematic owing to finite grid size (i.e., windowing effects). The ensemble-averaged (51 images) second-order structure functions for longitudinal velocity $S_2(r) = \langle\{[\mathbf{v}(\mathbf{x}+\mathbf{r}) - \mathbf{v}(\mathbf{x})]\cdot\hat{\mathbf{r}}\}^2\rangle$, vorticity $W_2(r) = \langle[\omega(\mathbf{x}+\mathbf{r}) - \omega(\mathbf{x})]^2\rangle$, and enstrophy flux $SW_2(r) = \langle|[\mathbf{v}(\mathbf{x}+\mathbf{r}) - \mathbf{v}(\mathbf{x})]\cdot\hat{\mathbf{r}}|\,[\omega(\mathbf{x}+\mathbf{r}) - \omega(\mathbf{x})]^2\rangle$ are shown in Fig. 4 for a downstream distance of 5 cm. Approximate slopes are shown as dashed lines in the graph. The slope in the real space of S_2 is about 1.6, corresponding to a -2.6 exponent in wave-number space compared to the predicted -3. The scaling exponent of W_2 is 0.4, corresponding to an exponent of -1.4 in wave-number space as opposed to the predicted -1.0. The latter difference is partly the result of computing W_2 on a finite grid as the slope increases from 0.4 to 0.6 and 1.3 for subsequent doublings of the grid spacing used for computing W_2. Thus, our measurement of an exponent of -1.4 is an upper bound and explains, in part, the results of Kellay *et al.* [7], where the single-point vorticity probe had a spatial resolution of about 2.5 times our grid spacing.

Perhaps the most interesting result of our analysis is the scaling of the enstrophy flux for which an exact result exists [13]: $\langle[\mathbf{v}(\mathbf{x}+\mathbf{r}) - \mathbf{v}(\mathbf{x})\cdot\hat{\mathbf{r}}][\omega(\mathbf{x}+\mathbf{r}) - \omega(\mathbf{x})]^2\rangle \sim 2\eta r$, where η is the enstrophy decay rate. This is the analog of the famous $4/5$ law of the third velocity moment in 3D turbulence which comes from the corresponding energy flux condition. In Fig. 4, the data for $SW_2(r)$ scale very closely as r with a constant factor which gives a measure of the enstrophy decay rate $\eta \approx 6\times 10^5\ \mathrm{s}^{-3}$. The relation for the dissipation scale $l_d = (\nu^3/\eta)^{1/6}$ yields $l_d \approx 0.2$ mm—very consistent with our data. Despite the slightly different way we compute the enstrophy flux—using the absolute value of velocity differences to get better statistics—and recognizing that the theoretical relationship is only exact in the limits of infinite Reynolds number, the agreement is both reasonable and internally consistent with our other measurements.

There are still important issues to be addressed. The effects of air drag and thickness fluctuations have not been systematically explored which could be accomplished by varying the film vapor pressure and tilt angle. Also, these are relatively weak turbulent flows and, as such, caution is needed when comparing to asymptotic high Reynolds number theories. We hope that further work on this system using the tools described in this Letter will continue to clarify the turbulent dynamics of flowing soap films.

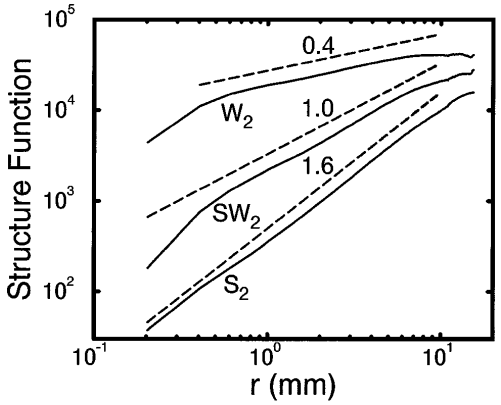

FIG. 4. Second-order structure functions S_2, W_2, and SW_2 vs r (solid lines) are labeled in the plot. Corresponding slopes are shown as dashed lines. For presentation purposes, S_2 and W_2 are scaled by 10 and 0.02, respectively.

We acknowledge useful discussions with S. Chen, A. Belmonte, R. Kraichnan, M. Rutgers, X.-L. Wu, and W. Goldburg. This work was funded by the U.S. Department of Energy.

*Permanent address: Dept. of Physics and Astronomy, University of Pittsburgh, Pittsburgh, PA 15260.

[1] Y. Couder, J. Phys. Lett. **45**, 353 (1984); Y. Couder, J. M. Chomaz, and M. Rabaud, Physica (Amsterdam) **37D**, 384 (1989).
[2] For reviews, see R. Kraichnan and D. Montgomery, Rep. Prog. Phys. **43**, 547 (1980); M. Lesieur, *Turbulence in Fluids* (Kluwer, Dordrecht, 1997).
[3] G. Batchelor, Phys. Fluids Suppl. **II**, 233 (1969).
[4] R. Kraichnan, Phys. Fluids **10**, 1417 (1967).
[5] M. Gharib and P. Derango, Physica (Amsterdam) **37D**, 406 (1989).
[6] H. Kellay, X.-L. Wu, and W. Goldburg, Phys. Rev. Lett. **74**, 3975 (1995).
[7] H. Kellay, X.-L. Wu, and W. Goldburg, Phys. Rev. Lett. **80**, 277 (1998).
[8] J. Chomaz and B. Cathalau, Phys. Rev. A **41**, 2243 (1990).
[9] J. McWilliams, J. Fluid Mech. **219**, 361 (1990).
[10] M. Rutgers, X.-L. Wu, A. P. R. Bagavatula, and W. Goldburg, Phys. Fluids **8**, 2847 (1997).
[11] VISIFLOW Analysis System. Copyright © AEA Technology (1987–1996).
[12] J. Chasnov, Phys. Fluids **9**, 171 (1997).
[13] A. Polyakov, Nucl. Phys. **B396**, 367 (1993); G. L. Eyink, Phys. Rev. Lett. **74**, 3800 (1995).